Sarcoplasmic reticulum Ca^{2+} handling in young DBA/2J vs C57BL/10 mdx models of Duchenne muscular dystrophy

Riley EG Cleverdon[1,2], Kennedy C Whitley[1,2], Daniel M Marko[3], Sophie I Hamstra[1,2], Jessica L Braun[1,2], Brian D Roy[1,2], Rebecca EK MacPherson[3,4], Val A Fajardo[1,2,4]*

[1] Department of Kinesiology, Brock University, St. Catharines, Ontario, Canada.
[2] Centre for Bone and Muscle Health, Brock University, St. Catharines, Ontario, Canada.
[3] Department of Health Sciences, Brock University, St. Catharines, ON L2S 3A1, Canada.
[4] Centre for Neuroscience, Brock University, St. Catharines, ON L2S 3A1, Canada.

Corresponding author:
Val A. Fajardo, PhD
Assistant Professor
Department of Kinesiology
Brock University
1812 Sir Isaac Brock Way
L2S 3A1
vfajardo@brocku.ca

Summary (150 word max)

The DBA/2J (D2) *mdx* mouse has emerged as a more severe model of Duchenne muscular dystrophy when compared to the traditional C57BL/10 (C57) *mdx* mouse. Here, we questioned whether sarcoplasmic reticulum (SR) Ca^{2+} handling would differ in muscles from young D2 and C57 *mdx* mice. Our results show that only D2 *mdx* mice had impaired SR Ca^{2+} uptake; however, both D2- and C57 *mdx* mice had impairments in SR Ca^{2+} leak, which was associated with lowered ryanodine receptor content. To further examine the impairments in SR Ca^{2+}uptake, Ca^{2+}-dependent SERCA activity assays were performed which showed that only the D2 *mdx*, but not C57 *mdx* mice had drastic impairments in SERCA-mediated ATP hydrolysis. Further, D2 mice had greater activation of the Ca^{2+}-activated protease, calpain. Overall, our study demonstrates that that SR Ca^{2+} handling is impaired early on in the D2 *mdx* mouse, specifically at the level of the SERCA pump.

Keywords: SERCA, sarcolipin, muscular dystrophy, energy expenditure, RYR, calcium leak, reactive oxygen species, reactive nitrogen species

INTRODUCTION

Duchenne muscular dystrophy (DMD) is an X-linked recessive muscle wasting disease, affecting approximately 1 in 3,500 boys worldwide (1, 2). Symptoms of DMD typically begin at three or four years of age and with no cure to date, patients usually succumb to cardiorespiratory complications from the disease by the third or fourth decade of life (3–5). Caused by the complete loss of dystrophin, a protein that normally connects the cytoskeleton and extracellular matrix to the sarcolemma, DMD is characterized by excessive membrane tearing and myofibre damage/degeneration (6). Loss of dystrophin is the initial insult of DMD, however there are several secondary consequences of the disease including chronic inflammation, oxidative stress, and calcium (Ca^{2+}) overload (7). Combined, these processes ultimately lead to the pathological hallmarks of DMD which include degeneration, necrosis, and fatty and fibrotic replacement of muscular tissue (8).

Ca^{2+} is a potent signaling molecule largely responsible for excitation-contraction coupling (ECC) in skeletal and cardiac muscle. Two major Ca^{2+} regulatory proteins involved in muscle ECC are the ryanodine receptor (RyR) and sarco-endoplasmic reticulum ATPase (SERCA) pump, located in the sarcoplasmic reticulum (SR). RyR is responsible for the release of Ca^{2+} from the SR into the myoplasm, which initiates cross-bridge formation and force generation, whereas SERCA catalyzes the reuptake of Ca^{2+} into the SR to initiate muscle relaxation (9, 10). However, several studies have shown that if SR Ca^{2+} handling is dysregulated, Ca^{2+} can become chronically elevated in the myoplasm, leading to muscle damage and weakness. Indeed, impaired Ca^{2+} handling is a major part of the pathology in the muscles of patients living with DMD. The resulting Ca^{2+} overload exacerbates oxidative stress, inflammation, and cellular necrosis which in turn perpetuates dystrophic pathology (11, 12). Further, RyR and SERCA function are implicated in

dystrophic muscles. For example, RyR leak has been shown to occur in excessive amounts caused by both depletion of the channel stabilizer calstabin and elevated reactive oxygen and nitrogen species (RONS) modifications to RyR1 (13). SERCA has also been shown to have impaired maximal Ca^{2+} uptake in murine models of DMD (14). Like RyR1, SERCA dysfunction in dystrophic muscles can also be partly attributed to RONS stress leading to damaging protein modifications (15).

The C57BL/10ScSn-*Dmd*^{mdx}/J (C57 *mdx*) mouse, originally discovered in 1984, has served as the dominant *in vivo* model to study cellular mechanisms and potential therapies for DMD (16). However, with a mild dystrophic pathology that is slow to progress, researchers have sought out alternative models that may better recapitulate human DMD (17). For example, previous research has shown that SERCA pump function is more severely impaired in the *mdx*/utrophin double knockout mouse – a severe DMD mouse model where both dystrophin and its functional homolog utrophin are completely absent (14). While this suggests that Ca^{2+} dysregulation may also partly contribute to the worsened pathology and weakness observed in the double knockout mouse model, it is important to note that this model does not genotypically represent DMD. More recently, the traditional C57 *mdx* mouse was backcrossed onto a DBA/2J background, giving way to the D2.B10-*Dmd*^{mdx}/J (D2 *mdx*) mouse (18). Unlike the C57 *mdx* mouse, the D2 *mdx* mouse presents with a juvenile onset and more severe DMD pathology, including pronounced muscle weakness and damage, degeneration, fibrosis, necrosis, and inflammation (18–20). The underlying mechanisms behind the greater pathology displayed in D2 *mdx* mice compared to C57 *mdx* mice are still under investigation, though a recent report has implicated elevated TGF- β signalling (21). However, to our knowledge SR Ca^{2+} handling has yet to be characterized in the D2 *mdx* mouse. Therefore, we examined SR Ca^{2+} handling in 8-10-week-old D2 and C57 *mdx* mice. This cohort

was selected based on previous studies showing that D2 *mdx* mice at this age display muscle weakness and pathology whereas the C57 *mdx* mice do not (18–20). We hypothesized that severity in pathology related to weakness observed in D2 *mdx* mice compared to the C57 *mdx* mice would be associated with greater impairments to SR Ca^{2+} handling.

RESULTS

Muscle weakness and wasting in the C57 mdx versus D2 mdx mice

We first sought to verify the phenotypical weakness and atrophy previously reported in the D2 *mdx* mice. As expected, serum CK was elevated in both *mdx* strains with a significant main effect of *mdx* genotype (Figure 1A). Moreover, gastrocnemius muscle and body mass were significantly lower in the D2 strain, with a significant interaction with *mdx* genotype indicating that body mass was lower in *mdx* vs WT mice, however only for the D2 *mdx* mouse (Figure 1B and C). When normalized to body mass, a significant main effect of strain was found suggesting that the gastrocnemius:body mass ratio was lower in D2 mice compare with C57 (Figure 1D). Holding impulse, or hangwire time normalized to body mass, was significantly lower across both *mdx* strains (Figure 1E). However, planned comparisons indicate that D2 *mdx* mice have less holding impulse compared with C57 *mdx* mice ($p < 0.05$, Student's t-test), consistent with previous reports of muscle weakness in the D2 *mdx* mice.

Metabolic phenotyping of the C57 mdx and D2 mdx mice

In further support of the apparent muscle weakness in the D2 *mdx* mice, metabolic cage data indicate that only the D2 *mdx* mice and not the C57 *mdx* mice were less ambulant in their cages (Figure 2A and B). We also found that the D2 *mdx* mice and not the C57 *mdx* mice had

elevated daily energy expenditure compared to WT (Figure 2C and D), with significant and trending reductions in food and water intake, respectively (Figure 2E-H). The Promethion metabolic cage system also allows for certain behavioural analyses including time spent in or touching its 'home' – a habitat enclosure on a slightly elevated platform. In both cases, we found that the D2 *mdx* mice spent less time in the habitat and interacting with the habitat compared to D2 WT mice, whereas these differences were not observed in the C57 *mdx* and C57 WT mice (Figure 2 I-L). We believe that this serves as an additional indication of muscle weakness, whereby the D2-*mdx* mice were not strong enough to enter the elevated enclosure.

SR Ca^{2+} uptake/filling and SERCA activity is impaired in D2 mdx mice but not C57 mdx mice

We then examined SR Ca^{2+} handling in gastrocnemius muscles from C57 and D2 -WT and -*mdx* mice (Figure 3). SR Ca^{2+} uptake experiments revealed impairments in the D2 *mdx* mice compared with WT mice but not C57 *mdx* mice (Figure 3A). A significant main effect of *mdx* genotype was found with starting $[Ca^{2+}]_{free}$ likely reflective of the Ca^{2+} overload present in the *mdx* muscles. However, a significant interaction revealed that only the D2 *mdx* muscles had elevated starting $[Ca^{2+}]_{free}$ compared with D2 WT as this was not observed in the C57 strain (Figure 3B). Similarly, AUC calculated from the Ca^{2+} uptake curves revealed a significant main effect of *mdx* genotype with AUC being higher in the *mdx* mice. However, a significant interaction indicated that this was only statistically significant for D2 WT vs D2 *mdx* and not C57 WT vs C57 *mdx* (Figure 3C). In addition, while maximum rates of Ca^{2+} uptake did not differ from C57 WT, C57 *mdx* and D2 WT mice we were unable to obtain a viable rate for D2 *mdx* mice (Figure 3D). When cyclopiazonic acid (CPA) was added to induce Ca^{2+} leak, we found that both D2- and C57 *mdx* mice had significantly lower Ca^{2+} leak with a significant main effect of *mdx* when AUC was

assessed (Figure 3E and F). To further explore the impairments in Ca^{2+} uptake, we then measured Ca^{2+}-dependent SERCA ATPase activity in the gastrocnemius muscle (Figure 3G and H). We found a trending interaction (p = 0.058) between *mdx* and strain indicating that maximal SERCA activity was impaired in gastrocnemius muscles from D2 *mdx* mice compared with D2 WT, but this was not observed in the C57 *mdx* and WT mice (Figure 3I). No changes in SERCA's apparent affinity for Ca^{2+} (pCa_{50}) were found (Figure 3J). Together, our Ca^{2+} uptake and SERCA activity findings demonstrated defective SR Ca^{2+} handling only in the D2 *mdx* mice. To determine a potential pathological consequence of Ca^{2+} dysregulation calpain activity was measured in the gastrocnemius. We found that calpain activity was higher in the *mdx* strains compared with their respective WTs, and that D2 mice generally had greater calpain activity compared to C57 mice (Figure 3K). Furthermore, planned comparisons between D2 *mdx* and C57 *mdx* showed that calpain activity was significantly higher in D2 *mdx* mice ($p = 0.0006$, Student's t-test).

Elevated RONS may contribute to impaired SR filling

To examine the potential mechanisms explaining the defective SR Ca^{2+} handling in D2 *mdx* mice, we performed western blotting of SR Ca^{2+} handling proteins (Figure 4). Our results showed that SERCA1 content was upregulated in both *mdx* strains (Figure 4A and B). SERCA2 content was upregulated in the *mdx* strains, however, a significant interaction indicated that this was only in the D2 *mdx* mice (Figure 4A and C). Sarcolipin (SLN) is a known inhibitor of SERCA that is upregulated in *mdx* mice (22) and was ectopically expressed in both the D2 *mdx* and C57 *mdx* gastrocnemius muscle; however, C57 *mdx* mice had a significantly higher content compared with D2 *mdx* (Figure 4D). RyR1 content was also altered with a trending main effect of strain showing lower RyR1 in D2 mice compared with C57 mice; and a significant main effect of *mdx*

genotype showing reduced RyR1 content in *mdx* mice (Figure 4E). Calstabin, the channel stabilizer of RyR1 did not have any significant changes in protein content (Figure 4F). We also investigated protein nitrosylation and nitration in the gastrocnemius under reducing conditions to determine levels of irreversible ROS modification. Our results show that D2 *mdx* mice but not C57 *mdx* mice have large amounts of cysteine adduction and tyrosine nitration (Figure 4G and H).

SR Ca^{2+} filling is also impaired in D2 mdx left ventricle and diaphragm muscles

Given the cardiorespiratory implications of DMD, we also assessed SR Ca^{2+} handling in cardiac (left ventricle) and diaphragm muscles from C57 and D2 -WT and -*mdx* mice. Similar to our results with the gastrocnemius, we found that D2 *mdx* mice had severe decrements in Ca^{2+} uptake in both the cardiac and diaphragm muscles (Figure 5). In the cardiac muscle, we found that starting $[Ca^{2+}]_{free}$ was trending higher in the D2 *mdx* vs D2 WT, while this was not observed in the C57 mice (Figure 5A and B). In addition, AUC was significantly higher in the D2 *mdx* vs D2 WT, and this again was not observed in the C57 mice (Figure 5C). Though there were no differences, apart from a main effect of strain on starting $[Ca^{2+}]_{free}$ in the diaphragm, a significant interaction was again detected with AUC analysis, with only D2 *mdx* mice having significantly elevated AUC, and thus impaired Ca^{2+} uptake vs D2 WT mice (Figure 5 D-F).

DISCUSSION

To our knowledge, this study is the first to compare SR Ca^{2+} handling in both the D2 *mdx* mouse and C57 *mdx* mouse. The D2 *mdx* mouse is known as a more severe DMD model with early onset weakness compared to the C57 *mdx* mouse. Impulse and measures of cage ambulation supported this showing that D2 *mdx* mice had early on-set muscle weakness occurring at 8-10 weeks of age. Also, the D2 *mdx* mice had less interaction with the elevated mouse home enclosure

compared to C57 *mdx* mice, suggesting that these mice were less able to jump onto this raised platform found within their cages. Interestingly, D2 *mdx* mice also had a hypermetabolic profile, where these mice had the highest levels of energy expenditure while ambulating the least, which we believe can contribute to the smaller body and muscle mass commonly observed in these mice. Perhaps inconsistent with our results, Strakova et al. (2018) found that energy expenditure was elevated in 5 month old C57 *mdx* mice compared with WT mice (23). We believe that this discrepancy could possibly be explained by age differences, as our C57 *mdx* mice were younger as compared to the mice used in the study by Strakova and colleagues.

To explain why the D2 *mdx* mice are much weaker at an earlier age, we explored the involvement of SR Ca^{2+} handling and any potential disturbances. Our Ca^{2+} uptake results showed that D2 *mdx* muscles (gastrocnemius, cardiac and diaphragm) had impaired ability to bring Ca^{2+} into the SR. This manifested as an elevated starting $[Ca^{2+}]_{free}$ and AUC during the uptake period. Since we did not add any exogenous Ca^{2+} to our experiments, we believe that the starting $[Ca^{2+}]_{free}$ is reflective of the Ca^{2+} overload known to be present in *mdx* muscles. That is, when the muscles are homogenized, there is an initial release of SR Ca^{2+} stores that must be rectified by the SERCA pumps. Thus, a higher starting $[Ca^{2+}]_{free}$ may already be reflective of impaired SERCA-mediated Ca^{2+} uptake, even before initiating the reaction with ATP. Subsequently and upon the addition of ATP, it was clear that the ability to remove cytosolic Ca^{2+} was impaired in D2 *mdx* (not C57 *mdx*) muscles leading to a larger AUC. Interestingly, in our hands this impairment in Ca^{2+} uptake was not associated with enhanced SR Ca^{2+} leak, as both D2- and C57 *mdx* mice actually had lower levels of Ca^{2+} leak upon the addition of CPA in our assay. A significant main effect of lowered RyR content in both D2- and C57 *mdx* muscles likely explains why there was less Ca^{2+} leak in these muscles.

To further explore the impairments in SR Ca^{2+} uptake, we conducted Ca^{2+}-dependent SERCA activity assays. Our results show that maximal SERCA activity in the gastrocnemius was impaired in D2 *mdx* but not C57 *mdx* mice compared with their respective WT groups, which could contribute to the overall impairments in SR Ca^{2+} uptake observed in D2 *mdx* mice. Collectively, these findings clearly show that SR Ca^{2+} dysregulation is present in young D2 *mdx* mice but not C57 *mdx* mice, which we believe ultimately contributes to the early-onset weakness and sets these mice on a worsened trajectory for aging. Further, SR Ca^{2+} dysregulation in the D2 *mdx* muscles may be a contributing factor to the elevated daily energy expenditure seen in the metabolic caging data. Considering the large reductions in cage ambulation, a high demand on Ca^{2+} regulation may contribute to the heightened energy expenditure in the D2 *mdx* mice. Since intracellular Ca^{2+} is high in these mice, as indicated with a higher starting $[Ca^{2+}]_{free}$ it is presumed that SERCA would be consuming a large amount of energy to try and limit myoplasmic Ca^{2+} levels in the D2 *mdx* muscles. Further, while SERCA activity was impaired in the D2 *mdx* mouse, there still was an appreciable amount of SERCA-mediated ATP hydrolysis. Combined with the result showing an inability to bring Ca^{2+} into the SR, our results suggest that the SERCA pumps have become highly inefficient – hydrolyzing ATP while bringing only minimal levels of Ca^{2+} into the SR. This uncoupling effect could also contribute to the elevated daily energy expenditure found in the D2 *mdx* mice.

The alterations to SERCA pump function do not seem to be explained by differences in SERCA protein levels. Both SERCA1 and SERCA2 were upregulated in the gastrocnemius, which we believe is an adaptive response aimed at improving SR Ca^{2+} handling. Indeed, SERCA density is an important determinant of SR Ca^{2+} filling, at least in healthy conditions (24, 25). However, any compensatory increase in SERCA content/density was unsuccessful in the rescuing SR Ca^{2+}

handling in D2 *mdx* mice. We next examined SLN expression. Although it is not typically expressed in murine gastrocnemius muscle, ectopic expression of SLN occurred in both *mdx* mouse models, with SLN protein being elevated to a greater extent in the C57 *mdx* mice compared to the D2 *mdx* mice. Studies have shown that SLN is upregulated along with disease progression with its expression being further upregulated in the *mdx*/utrophin double knockout mice compared with *mdx* mice (14). Knocking out SLN in these mice improved dystrophic pathology suggesting that SLN may contribute to *mdx* pathology. However, there are discrepant results with SLN deletion studies also impairing *mdx* pathology or not changing the phenotype (26). Since we found that SLN was less upregulated in the more severe D2 *mdx* mouse model with dramatic impairments in SERCA function, our results could suggest that SLN may not be a critical player in the SERCA function impairments and potentially *mdx* pathology in the D2 *mdx* mouse; however, this should be investigated further specifically in the D2 *mdx* mouse. In addition, SLN is a known uncoupler of SERCA and its upregulation in the D2 *mdx* mouse may contribute to the observed increase in daily energy expenditure (27–29). However, even though SLN was more upregulated in C57 *mdx* mice, these mice did not show elevated energy expenditure compared with C57 WT mice. Thus, alternative mechanisms may be contributing to the increased energy expenditure. One potential factor may be elevated oxidative/nitrosative stress. SERCA is susceptible to RONS damage and RONS are known to be high in DMD, and therefore, it is plausible that RONS modifications could be contributing to the changes in SERCA function (15, 30–34). Our results of elevated total protein nitrosylation and tyrosine nitration under reducing conditions are suggestive of irreversible RONS modifications that may be impairing the SERCA pump. Moreover, damage to the SR membrane itself from RONS may contribute to impairments in SR Ca^{2+} filling by leaking Ca^{2+} out during the uptake period, altogether contributing to the apparent inefficiencies of the pump.

We also determined the activation of calpain in D2 *mdx* gastrocnemius muscles. Calpain is a Ca^{2+}-dependent proteolytic enzyme previously shown to be more active in *mdx* muscles (35). To our knowledge, ours is the first study to demonstrate that rates of calpain activity are higher in the D2 background compared to C57, irrespective of the *mdx* genotype. Furthermore, planned comparisons between D2 *mdx* and C57 *mdx* reveals a significant 2.2-fold increase in calpain activity in the former vs the latter ($p = 0.0006$ via Student's t-test). This finding is important and adds mechanistic insight that may partly explain the worsened pathology in the D2 *mdx* mouse. It is interesting that the D2 WT mice already had elevated calpain activation compared with C57 WT. This apparent difference in background strain may provide additional insight as to why *mdx* mice on the D2 background are worse off than *mdx* mice on the C57 background. One explanation that is not yet well understood, is a potential crosstalk between calpain activation and the pro-fibrotic factor TGF-β. Previous studies have found that TGF-β1 upregulation in lung fibroblasts and atrial derived myocytes can increase calpain activation (36, 37). This is interesting given recent findings showing that a polymorphism of LTBP4 in D2 WT mice greatly upregulates TGF-β (38), suggesting that the increased TGF-β activity could increase calpain activity in the D2 WT mice. This combined with the impairments observed in SERCA function could contribute to elevated calpain in the D2 *mdx* mice.

In conclusion, our study clearly shows impairments in SR Ca^{2+} handling in skeletal and cardiac muscles from D2 *mdx* mice, particularly at the level of the SERCA pump. Our results suggest that the early onset weakness and damage observed in young D2 *mdx* mice may be partly due to an inability to bring Ca^{2+} into the SR. Future studies should investigate whether improving SERCA function, potentially through cytotoxic protection against RONS may mitigate dystrophic pathology and improve physiological outcomes in the D2 *mdx* mouse.

LIMITATIONS TO THE STUDY

Our study clearly shows that SERCA function is impaired early on in D2 *mdx* mice and may contribute to the severity of muscle weakness and damage. However, we acknowledge that our work is largely descriptive, and future studies aimed at improving SERCA function will determine its causal role, if any. Furthermore, the mechanisms leading to these impairments in SERCA function are still unknown, though we associate them with elevated oxidative/nitrosative stress. Our study is also limited in that we are unable to pinpoint the source of the oxidative/nitrosative stress. We speculate that high intracellular Ca^{2+} can lead to mitochondrial dysfunction in DMD pathology and may be an additional contributing factor of Ca^{2+}-related pathology. Elevated myoplasmic Ca^{2+} can increase intake of Ca^{2+} into the mitochondria which eventually leads to the opening of the mitochondrial permeability transition pore (mPTP), then swelling and bursting of the mitochondria, excessive H_2O_2 emission into the myoplasm, and subsequent calpain activation (39). A recent study by Hughes and colleagues indeed found that D2 *mdx* mice have a greater number of swollen mitochondria, increased susceptibility to mPTP opening in the quadriceps and excessive H_2O_2 emission (40). This could be contributing to the increased RONS released into the muscle and subsequent SR Ca^{2+} handling dysfunction. Furthermore, the impairments in SR Ca^{2+} handling could be perpetuating the mitochondrial dysfunction occurring in the D2 *mdx* mice, thereby creating a vicious cycle leading to muscle degeneration and weakness. Finally, our study does not discern whether the elevated daily energy expenditure in D2 *mdx* mice is caused solely by increased muscle-based energy consumption. Other thermogenic organs such as brown and beige fat could be investigated in the future.

ACKNOWLEDGEMENTS

This work was supported by an unrestricted Brock University internal grant and a Canada Research Chair Tier 2 in Tissue Plasticity and Remodelling to VAF. REGC and SIH were supported by a NSERC CGS-M, and JLB was supported by a CIHR CGS-M.

AUTHOR CONTRIBUTIONS

Riley EG Cleverdon: Conceptualization, methodology, validation, formal analysis, investigation, writing – original draft, visualization

Kennedy C Whitley: Methodology, investigation, formal analysis, writing – review & editing

Daniel M Marko: Methodology, investigation, formal analysis, writing – review & editing

Sophie I Hamstra: Investigation, formal analysis, writing – review & editing

Jessica L Braun: Investigation, formal analysis, writing – review & editing

Brian D Roy: Resources, writing – review & editing

Rebecca EK MacPherson: Resources, supervision, writing – review & editing

Val A Fajardo: Conceptualization, supervision, project administration, funding acquisition, investigation, formal analysis, visualization, writing – original draft

DECLARATION OF INTERESTS

The authors declare no competing interests.

FIGURE LEGENDS

Figure 1: Creatine kinase, muscle/body mass and impulse: A) Serum creatine kinase activity expressed in units per litre. B) Gastrocnemius mass (mg), C) body mass (g), and D) gastrocnemius mass:body mass ratio (mg:g). E) Impulse expressed as hangwire time*body mass. A two-way ANOVA was used for all comparisons, n=12 per group. Values are represented as mean ± SEM. Main effects and interactions expressed in bars over the graph, ****$p < 0.0001$ using a Sidak's post-hoc test.

Figure 2. Cage activity, energy expenditure and cage behaviour: A) Daily cage ambulation in D2 mice and B) C57 mice expressed in metres travelled. C) Energy expenditure in D2 mice and D) C57 mice expressed in kcal/kg of body mass/hr. E) and G) Food (g) and water (mL) intake of D2 mice and F) and H) C57 mice. Percentage of time spent in (I-Home) and interacting with (T-Home) the mouse home for D2 mice I) and K) and C57 mice J) and L). All metabolic cage analyses were measured over a 48-hour period. Two-way repeated ANOVA examining the effect of time period, *mdx* genotype and their potential interaction (A-H). **$p < 0.01$, *** $p < 0.001$, and ****$p < 0.0001$ using a Sidak's post-hoc test, n = 5-6 per group. Student's t-test examined WT versus mdx (I-L), n = 5-6 per group. Values are represented as mean ± SEM.

Figure 3: SR Ca^{2+} uptake/leak, SERCA and calpain activity in C57 and D2 -WT and -*mdx* gastrocnemius muscle: A) Ca^{2+} uptake curves from gastrocnemius homogenates. B) Starting $[Ca^{2+}]_{free}$ levels immediately after ATP addition. C) Area under the curve (AUC) of Ca^{2+} uptake curves. D) Maximum rate of Ca^{2+} uptake obtained from the Ca^{2+} uptake curves expressed as nmol/g of protein/min. E) Ca^{2+} leak curve after the addition of cyclopiazonic acid (CPA) and expressed as the change relative to baseline Ca^{2+} immediately after CPA addition. The addition of CPA inhibits the SERCA pump allowing for SR Ca^{2+} to be released back into the cytosol. F) AUC analysis of SR Ca^{2+} leak. G) & H) Ca^{2+}-dependent SERCA activity curves in D2 and C57 -WT and -*mdx* gastrocnemius muscles. I) Maximal SERCA activity expressed as μmol/g of protein/min and J) pCa_{50} of SERCA activity, n = 4. K) Calpain activity in gastrocnemius muscles from D2 and C57 -WT and -*mdx* gastrocnemius muscles expressed as RFU min/mg of protein. Two-way ANOVAs were performed with a Sidak's post-hoc test, *$p < 0.05$, **$p < 0.01$, ***$p < 0.001$, and ****$p < 0.0001$ n= 5-6. Main effects and interactions expressed in bars over the graph. Values are represented as mean ± SEM.

Figure 4: Western blot analyses of SR Ca^{2+} handling proteins total protein nitrosylation and tyrosine nitration: A) Representative Western blot images for SERCA1 and SERCA2 and their respective semi-quantificational analyses in gastrocnemius muscles from D2 and C57 -WT and *mdx* mice (B and C). D) SLN content in gastrocnemius muscles. E) RyR1 and F) calstabin content in gastrocnemius muscles from D2 and C57 -WT and -*mdx*. G) Protein nitrosylation measured via Western blotting for nitrocysteine-adducted protein. H) Protein tyrosine nitration measured via Western blotting for nitrotyrosine-adducted protein. For B,C and E-H, a two-way ANOVAs were performed with a Sidak's post-hoc test, **$p < 0.01$, ***$p < 0.001$, ****$p < 0.0001$ n = 6 per group. Main effects and interactions expressed in bars over the graph. For D a Student's t-test was used, *$p < 0.05$, n = 6 per group. All protein contents are expressed as arbitrary units. Values are represented as mean ± SEM.

Figure 5: Ca^{2+} uptake in the cardiac and diaphragm muscles: A) Ca^{2+} uptake curves from left ventricle homogenates. B) Starting $[Ca^{2+}]_{free}$ levels immediately after ATP addition and C) AUC analysis in left ventricle homogenates. D) Ca^{2+} uptake curves from diaphragm homogenates. E) Starting $[Ca^{2+}]_{free}$ levels immediately after ATP addition and F) AUC analysis in diaphragm homogenates. Two-way ANOVAs were performed with a Sidak's post-hoc test, ****$p < 0.0001$, n= 5-6. Main effects and interactions expressed in bars over the graph. Values are represented as mean ± SEM.

STAR Methods

RESOURCE AVAILABILITY

Lead contact

Further information and requests for resources and reagents should be directed to and will be fulfilled by the lead contact, Val A. Fajardo (vfajardo@brocku.ca).

Materials availability

This study did not generate new unique reagents.

Data and code availability

All data are included in the published article or are available from the lead contact upon reasonable request. This paper does not report original code.

EXPERIMENTAL MODELS AND SUBJECT DETAILS

Mice and Design

Male C57 *mdx* (n = 12), C57 WT (n = 12), D2 *mdx* (n = 12), and D2 WT (n = 12) mice were purchased from Jackson Laboratories at 7-8 weeks of age. They were acclimated and housed in Brock University's Animal Facility, in an environmentally controlled room with a standard 12:12 hour light-dark cycle and allowed access to food and water *ad libitum*. After the mice reached 9-10 weeks of age, they were euthanized via cervical dislocation under general anesthetic (vaporized isoflurane) and their tissues were collected.

METHOD DETAILS

Hang Wire Testing

At 8-9 weeks of age, mice were subjected to a hang wire test to determine limb strength and endurance. All mice were gently placed on the wire situated 12 inches high and were left suspended on the wire until they reached exhaustion and dropped from the wire to the base of the cage. The time they remained suspended was recorded for three trials, separated by a 60s recovery period. Impulse (s*g) was calculated according to DMD_M.2.1.004 standard operating procedures by multiplying the average time suspended by body mass.

Metabolic Caging

At 8-9 weeks of age, mice were housed in pairs in a Promethion Metabolic Cage System for 48 hours. Two 12-hour light and dark cycles were measured, and data was collected. Food and water intake were measured through mass changes with the MM-1 load cell, the Promethion mass measurement device. Cage ambulation was quantified through metres travelled which is collected through beam breaks with the BXYZ Beambreak Activity Monitor in the x y, and z planes. Respiratory exchange ratio (RER) was calculated as VCO_2 (volume of carbon dioxide expired each minute) divided by VO_2 (volume of oxygen inspired each minute) measured from the Promethion metabolic cages equipped with O_2 and CO_2 gas analyzers. To obtain mean energy expenditure expressed in kcal/hr, the Weir equation was used (41).

Sample Collection and Homogenization

Gastrocnemius, diaphragm, and cardiac muscles (n=12/group) were rapidly extracted from euthanized animals and flash frozen in liquid N2 and stored at -80˚C. For Ca^{2+} uptake and SERCA

activity analyses, muscles were homogenized in homogenizing buffer (5 mM HEPES, 250 mM sucrose, 0.2 mM PMSF, 0.2% NaN3; pH 7.5). An aliquot of the muscle homogenate was then supplemented with protease and phosphatase (phosSTOP; cOmplete Mini) inhibitors for western blot analyses. Blood was collected via cardiac puncture and spun at 5000 x g for 8 minutes (4°C) and serum was collected and stored at -80˚C.

Serum Creatine Kinase Activity

Serum creatine kinase activity was determined as previously described (42), with a M2 Molecular Device plate reader and a commercially available assay (Cat. #C7522, Pointe Scientific Inc., Canton, MI, USA) fitted onto a 96-well plate and calibrated with a standard curve of purified creatine kinase (Sigma, Oakville, ON, Canada, Cat. 10127566001).

Sarcoplasmic Reticulum Ca^{2+} Uptake and Leak

Ca^{2+} uptake assays were fitted onto a 96-well plate and done on a M2 Molecular Device plate reader and the ratio-able Ca^{2+} fluorescent indicator Indo-1. In brief, 20 μl of diaphragm, 25 μl of gastrocnemius or 50 μl of left ventricle homogenate was added to 200 μl Ca^{2+} uptake buffer (20mM HEPES, 200mM KCL, 10mM NaN_3, 5μM TPEN, 15mM $MgCl_2$, 5mM Oxalate; pH 7.0), and 1 μl of Indo-1 (1 mM in 50 mM glycine, pH 7.0). Ca^{2+} uptake was initiated with 4 μl of ATP (250 mM, pH 7.0) with the plate read kinetically set with an excitation wavelength of 355 nM and emission wavelengths of 405 nm (Ca^{2+}-bound Indo-1) and 485 nm (Ca^{2+}-free Indo-1). After the plateau was reached, 1 μl of cyclopiazonic acid (CPA) was added to inhibit the SERCA pump and initiate SR Ca^{2+} leak. The plate was then read for an additional 600s. Free Ca^{2+} concentration was calculated using the following formula and a Kd of 250 nM for Indo-1. The amount of Ca^{2+} uptake

and leak were measured through an area under the curve analysis (AUC). In addition, rates of Ca^{2+} uptake and leak were analyzed and normalized to grams of protein measured by a BCA assay.

$$[Ca^{2+}] = K_d \left(\frac{R - R_{min}}{R_{max} - R}\right)\left(\frac{S_{f2}}{S_{b2}}\right)$$

Formula 1: Free Calcium Concentration ($[Ca^{2+}]_f$)
K_d is the dissociation constant of Indo-1 (250 nM). R_{min} refers to the ratio of bound:unbound Indo-1 after adding 15 mM EGTA. R_{max} refers to the ratio of bound:unbound Indo-1 after adding 5 M $CaCl_2$. S_{f2} is the fluorescence emission at 485nm (Ca^{2+}-free Indo-1) in the EGTA portion and S_{b2} is the fluorescence emission at 485nm in the 5 M $CaCl_2$ portion.

SERCA ATPase Activity

Ionophore (A23187; Sigma Aldrich) supported SERCA activity was measured in gastrocnemius homogenates using an enzyme-linked spectrophotometric assay as previously described (24, 30, 43). Briefly, muscle homogenates (15 μl), pyruvate kinase (PK) and lactate dehydrogenase (LDH) (18 U I^{-1} for both) were added to Ca^{2+} ATPase buffer (20mM HEPES, 200mM KCl, 10mM NaN3, 1mM EGTA, 15mM MgCl2, 5mM ATP, 10mM phosphoenolpyruvate). To initiate SERCA activity, 4 μl of 1.9% (w/v) NADH was added and the plates were then read at 340 nm for 30 minutes. SERCA-dependent activity in gastrocnemius homogenates was calculated with a pathlength correction, extinction coefficient of NADH (6.22 mM), and the subtraction of ATPase activity in the presence of 1 μl SERCA-specific inhibitor, CPA (40 mM) from total ATPase activity across a range of Ca^{2+} concentrations (*p*Ca 6.95 – 5.75). A bicinchoninic acid (BCA) assay was done to normalize SERCA activity to grams of protein.

Western Blotting

Western blotting was conducted to determine protein expression of SERCA1a/2a, sarcolipin (SLN), RyR1 and calstabin. Laemmli buffer was added to muscle homogenates to

solubilize proteins that were then electrophorectially separated at 240V for 22 minutes on a 7-12% TGX gradient gel (BioRad). Proteins were transferred to PVDF or nitrocellulose membranes for 6 minutes using BioRad Trans Blot Turbo. Prior to blocking, SuperSignal western Blot Enhancer (46641) from Thermo Scientific was applied for the SLN blot. A 5% (w/v) milk and TBST solution was used to block the membranes for one hour. Primary antibody was then added and incubated overnight at 4°C. The primary antibodies SERCA1a (MA3-911), SERCA 2a (MA3-919), RYR1 (MA3-925) and calstabin (PA1-026A) were obtained from ThermoFisher Scientific (Waltham, MA, USA). The primary antibody for SLN (ABT13) was obtained from Sigma-Aldrich (Oakville, ON, CA). The primary antibody for nitrocysteine (ab94930) was obtained from Abcam (Cambridge, UK). The primary antibody for nitrotyrosine (189542) was obtained from Cayman Chemical (Ann Arbor, MI, USA). Subsequent to primary incubation, the membranes were washed three times with TBST and then incubated with anti-mouse (SERCA1a/2a, RyR1 ;7076; Cell Signalling Technology) or anti-rabbit (calstabin, SLN; 7074, Cell Signalling Technology,) secondary antibodies at room temperature for 1 hour. The membranes were then washed again three times with TBST then chemiluminescent substrate Millipore Immobilon (WBKLS0500; Sigma-Aldrich) or SuperSignal West Femto Maximum Sensitivity Substrate (34095; Thermo Scientific) was added prior to imaging with a BioRad Chemidoc. Optical densities were analyzed with imageLab (BioRad) and normalized to total protein visualized with a ponceau stain (59803; Cell Signalling Technology).

Calpain Activity Assay

A commercialized calpain assay (QIA120; Millipore Sigma) was used in order to determine calpain activity in the gastrocnemius. Tissue was freshly homogenized in RIPA lysis

buffer and 50 μl of sample was loaded in duplicate in either 100 μl of activator buffer or 100 μl of inhibitor buffer in a 96-well plate as per the manufacturer's instructions. Then, 50 μl of diluted substrate was added in the dark into each well and the plate was incubated for 15 minutes. The plate was then measured for 10 minutes as a kinetic plate at an excitation of 370 nm and emission of 450 nm to determine the rate of calpain activity normalized to total protein (via BCA assay).

Ethics statement

All animal procedures were approved by the Brock University Animal Care and Utilization Committee (file #17-06-03) and were carried out in accordance with the Canadian Council on Animal Care guidelines.

QUANTIFICATION AND STATISTICAL ANALYSIS

Statistical analysis

A two-way ANOVA was used to test the main effects of genotype (*mdx*) and strain (C57 or D2) and their potential interaction for most analyses. Post-hoc testing was completed using Sidak multiple comparison testing. A Student's t-test was also used to compare cage ambulation data. Statistical tests were conducted using GraphPad Prism 8 Software (San Diego, USA). All values are presented as means ± standard error. Statistical significance is set to $p \leq 0.05$.

References

1. Moat SJ, Bradley DM, Salmon R, Clarke A, Hartley, L. (2013) Newborn bloodspot screening for Duchenne muscular dystrophy: 21 years experience in Wales (UK). *Eur. J. Hum. Genet.* 2013;21(10): 1049–1053. doi: 10.1038/ejhg.2012.301.

2. Emery AE. (1991) Population frequencies of inherited neuromuscular diseases - a world survey. *Neuromuscul. Disord.* 1991;1(1):19–29. doi: 10.1016/0960-8966(91)90039-u.

3. Straub V, Balabanov P, Bushby K, et al. Stakeholder cooperation to overcome challenges in orphan medicine development: the example of Duchenne muscular dystrophy. *Lancet Neurol*. 2016;15(8):882–890. doi: 10.1016/S1474-4422(16)30035-7.

4. Emery AEH. The muscular dystrophies. *Lancet*. 2002;359(9307):687–695. doi: 10.1016/S0140-6736(02)07815-7.

5. Grigore I, Frasin M, Diaconu G. Cardiac complications in Duchenne muscular dystrophy in children. *Rev Pediatr Obstet Ginecol Pediatr*. 2015;64(4):5. doi: 10.37897/RJP.2015.4.4.

6. Blake DJ, Weir A, Newey SE, Davies KE. Function and Genetics of Dystrophin and Dystrophin-Related Proteins in Muscle. *Physiol Rev*. 2002;82(2):291–329. doi: 10.1152/physrev.00028.2001.

7. Tubridy N, Fontaine B, Eymard B. Congenital myopathies and congenital muscular dystrophies. *Curr. Opin. Neurol.* 2001;14(5):575–582. doi: 10.1097/00019052-200110000-00005.

8. Shin J, Tajrishi MM, Ogura Y, Kumar A. Wasting mechanisms in muscular dystrophy. *Int J Biochem Cell Biol*. 2013;45(10):2266–2279. doi: 10.1016/j.biocel.2013.05.001.

9. Santulli G, Lewis D, des Georges A, Marks AR, Frank J. Ryanodine Receptor Structure and Function in Health and Disease. *Subcell. Biochem.* 2018;87:329–352. doi: 10.1007/978-981-10-7757-9_11.

10. MacLennan DH, Rice WJ, Green NM. The Mechanism of Ca^{2+} Transport by Sarco(Endo)plasmic Reticulum Ca^{2+}-ATPases. *J. Biol. Chem.* 1997;272(46):28815–28818. doi: 10.1074/jbc.272.46.28815.

11. Turner PR, Westwood T, Regen CM, Steinhardt RA. Increased protein degradation results from elevated free calcium levels found in muscle from mdx mice. *Nature*. 1988;335 (6192):735–738. doi: 10.1038/335735a0.

12. Robert V, Massimino ML, Tosello V, Marsault, et al. Alteration in calcium handling at the subcellular level in mdx myotubes. *J. Biol. Chem.* 2001;276(7):4647–4651. doi: 10.1074/jbc.M006337200.

13. Bellinger AM, Reiken S, Carlson C, et al. Hypernitrosylated ryanodine receptor/calcium release channels are leaky in dystrophic muscle. *Nat Med*. 2009;15(3):325–330. doi: 10.1038/nm.1916.

14. Voit A, Patel V, Pachon R, et al. Reducing sarcolipin expression mitigates Duchenne muscular dystrophy and associated cardiomyopathy in mice. *Nat Commun*. 2017;8(1). doi: 10.1038/s41467-017-01146-7.

15. Gehrig SM, van der Poel C, Sayer TA, et al. Hsp72 preserves muscle function and slows progression of severe muscular dystrophy. *Nature*. 2012;484(7394):394–398. doi: 10.1038/nature10980.

16. Bulfield G, Siller WG, Wight PA, Moore KJ. X chromosome-linked muscular dystrophy (mdx) in the mouse. *Proc Natl Acad Sci U S A*. 1984;81(4):1189–1192. doi: 10.1073/pnas.81.4.1189.

17. Swiderski K, Lynch GS. Murine models of Duchenne muscular dystrophy: is there a best model? *Am J Physiol Cell Physiol*. 2021;321(2) doi: 10.1152/ajpcell.00212.2021.

18. Coley WD, Bogdanik L, Vila MC. et al. Effect of genetic background on the dystrophic phenotype in mdx mice. *Hum. Mol. Genet.* 2016;25(1):130–145. doi: 10.1093/hmg/ddv460.

19. Hammers DW, Hart CC, Matheny MK, et al. The D2.mdx mouse as a preclinical model of the skeletal muscle pathology associated with Duchenne muscular dystrophy. *Sci Rep*. 2020;10(1):14070. doi: 10.1038/s41598-020-70987-y.

20. van Putten M, Putker K, Overzier M, et al. Natural disease history of the D2-mdx mouse model for Duchenne muscular dystrophy. *FASEB J*. 2019;33(7):8110–8124. doi: 10.1096/fj.201802488R.

21. Mázala DAG, Novak JS, Hogarth MW, et al. (2020) TGF-β–driven muscle degeneration and failed regeneration underlie disease onset in a DMD mouse model. *JCI Insight*. 2020;5(6):e135703. doi: 10.1172/jci.insight.135703.

22. Schneider JS, Shanmugam M, Gonzalez JP, et al. Increased sarcolipin expression and decreased sarco(endo)plasmic reticulum Ca2+ uptake in skeletal muscles of mouse models of Duchenne muscular dystrophy. *J. Muscle Res. Cell. Motil.* 2013;34(5-6):349–356. doi: 10.1007/s10974-013-9350-0.

23. Strakova J, Kamdar F, Kulhanek D, et al. Integrative effects of dystrophin loss on metabolic function of the mdx mouse. *Sci Rep*. 2018;8(1):13624. doi: 10.1038/s41598-018-31753-3.

24. Hamstra SI, Kurgan N, Baranowski RW, et al. Low-dose lithium feeding increases the SERCA2a-to-phospholamban ratio, improving SERCA function in murine left ventricles. *Exp Physiol*. 2020;105(4):666–675. doi: 10.1113/EP088061.

25. Smith IC, Bombardier E, Vigna C, Tupling AR. ATP Consumption by Sarcoplasmic Reticulum Ca2+ Pumps Accounts for 40-50% of Resting Metabolic Rate in Mouse Fast and Slow Twitch Skeletal Muscle. *PLoS ONE*. 2013;8(7):e68924. doi: 10.1371/journal.pone.0068924.

26. Bal NC, Gupta SC, Pant M, et al. Is Upregulation of Sarcolipin Beneficial or Detrimental to Muscle Function? *Front Physiol*. 2021;12:633058. doi: 10.3389/fphys.2021.633058.

27. Smith WS, Broadbridge R, East JM, Lee AG. Sarcolipin uncouples hydrolysis of ATP from accumulation of Ca2+ by the Ca2+-ATPase of skeletal-muscle sarcoplasmic reticulum. *Biochem J*. 2002;361(2):277–286. doi: 10.1042/0264-6021:3610277.

28. Bombardier E, Smith IC, Vigna C, Fajardo VA, Tupling AR. Ablation of sarcolipin decreases the energy requirements for Ca2+ transport by sarco(endo)plasmic reticulum Ca2+-ATPases in resting skeletal muscle. *FEBS Lett*. 2013;587(11):1687–1692. doi: 10.1016/j.febslet.2013.04.019.

29. Mall S, Broadbridge R, Harrison SL, et al. The presence of sarcolipin results in increased heat production by Ca(2+)-ATPase. *J Biol Chem*. 2006;281(48):36597–36602. doi: 10.1074/jbc.M606869200.

30. Braun JL, Hamstra SI, Messner HN, Fajardo VA. SERCA2a tyrosine nitration coincides with impairments in maximal SERCA activity in left ventricles from tafazzin-deficient mice. *Physiol Rep*. 2019;7(16):e14215. doi: 10.14814/phy2.14215.

31. Fu M, Bombardier E, Gamu D, Tupling AR. Phospholamban and sarcolipin prevent thermal inactivation of sarco(endo)plasmic reticulum Ca2+-ATPases. *Biochem J*. 2020;477(21):4281–4294. doi: 10.1042/BCJ20200346.

32. Fajardo VA, Trojanowski N, Castelli LM, et al. Saturation of SERCA's lipid annulus may protect against its thermal inactivation. *Biochem Biophys Res Commun*. 2017;484(2):456–460. doi: 10.1016/j.bbrc.2017.01.154.

33. Fu MH, Tupling AR. Protective effects of Hsp70 on the structure and function of SERCA2a expressed in HEK-293 cells during heat stress. *Am. J. Physiol. Heart Circ. Physiol.* 2009;296(4):H1175-1183. doi: 10.1152/ajpheart.01276.2008.

34. Tupling AR. Protection of heart and skeletal muscle by heat shock proteins. *Appl Physiol Nutr Metab*. 2008;33(5):1021–1022. doi: 10.1139/H08-066.

35. Gailly P, De Backer F, Van Schoor M, Gillis JM. In situ measurements of calpain activity in isolated muscle fibres from normal and dystrophin-lacking mdx mice. *J Physiol*. 2007;582(3):1261–1275. doi: 10.1113/jphysiol.2007.132191.

36. Li F-Z, Cai P-C, Song L-J, et al. Crosstalk between calpain activation and TGF-β1 augments collagen-I synthesis in pulmonary fibrosis. *Biochim Biophys Acta Mol Basis Dis*. 2015;1852(9):1796–1804. doi: 10.1016/j.bbadis.2015.06.008.

37. Yeh Y-H, Kuo C-T, Chan T-H, et al. Transforming growth factor-β and oxidative stress mediate tachycardia-induced cellular remodelling in cultured atrial-derived myocytes. *Cardiovasc Res*. 2011;91(1):62–70. doi: 10.1093/cvr/cvr041.

38. Heydemann A, Ceco E, Lim JE, et al. Latent TGF-β–binding protein 4 modifies muscular dystrophy in mice. *J. Clin. Invest.* 2009;119(12):3703–3712. doi: 10.1172/JCI39845.

39. Timpani CA, Hayes A, Rybalka E. Revisiting the dystrophin-ATP connection: How half a century of research still implicates mitochondrial dysfunction in Duchenne Muscular Dystrophy aetiology. *Med Hypotheses*. 2015;85:1021–1033.

40. Hughes MC, Ramos SV, Turnbull PC, et al. Early myopathy in Duchenne muscular dystrophy is associated with elevated mitochondrial H2 O2 emission during impaired oxidative phosphorylation. *J Cachexia Sarcopenia Muscle*. 2019;10(6):643–661. doi: 10.1016/j.mehy.2015.08.015.

41. Weir JB de V. New methods for calculating metabolic rate with special reference to protein metabolism. *J Physiol*. 1949;109(1-2):1–9. doi: 10.1113/jphysiol.1949.sp004363.

42. McKinlay BJ, Theocharidis A, Adebero T, et al. Effects of Post-Exercise Whey Protein Consumption on Recovery Indices in Adolescent Swimmers. *IJERPH*. 2020(21);17:7761. doi: 10.3390/ijerph17217761.

43. Hamstra SI, Whitley KC, Baranowski RW, et al. The role of phospholamban and GSK3 in regulating rodent cardiac SERCA function. *Am. J. Physiol., Cell Physiol.* 2020;319(4). doi: 10.1152/ajpcell.00318.2020.

Figure 1

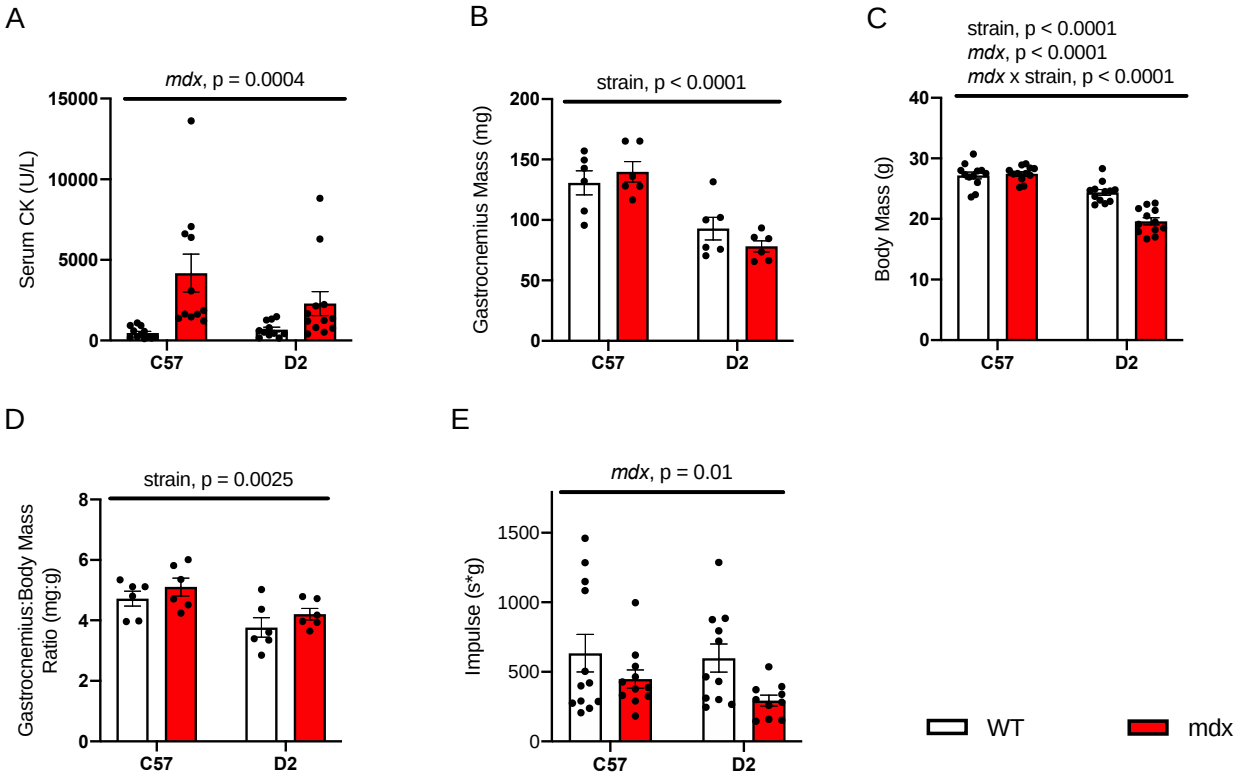
A
mdx, p = 0.0004
Serum CK (U/L)
15000
10000
5000
0
C57
D2
B
strain, p < 0.0001
Gastrocnemius Mass (mg)
200
150
100
50
0
C57
D2
C
strain, p < 0.0001
mdx, p < 0.0001
mdx x strain, p < 0.0001
Body Mass (g)
40
30
20
10
0
C57
D2
D
strain, p = 0.0025
Gastrocnemius:Body Mass Ratio (mg:g)
8
6
4
2
0
C57
D2
E
mdx, p = 0.01
Impulse (s*g)
1500
1000
500
0
C57
D2
WT
mdx

Figure 2

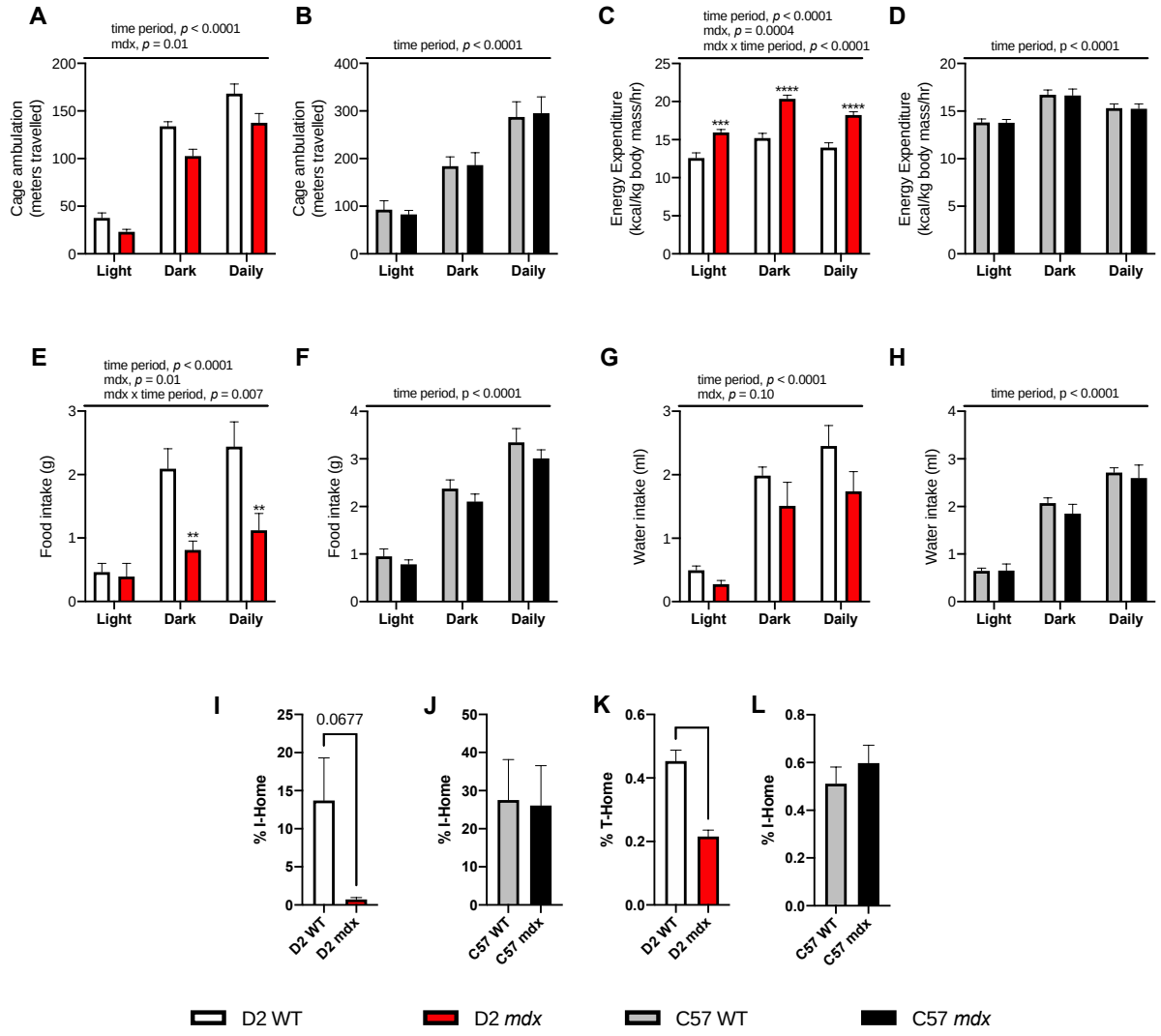
A
time period, p < 0.0001
mdx, p = 0.01
Cage ambulation (meters travelled)
Light
Dark
Daily
B
time period, p < 0.0001
Cage ambulation (meters travelled)
C
time period, p < 0.0001
mdx, p = 0.0004
mdx x time period, p < 0.0001
Energy Expenditure (kcal/kg body mass/hr)
***
****
****
D
time period, p < 0.0001
Energy Expenditure (kcal/kg body mass/hr)
E
time period, p < 0.0001
mdx, p = 0.01
mdx x time period, p = 0.007
Food intake (g)
**
**
F
time period, p < 0.0001
Food intake (g)
G
time period, p < 0.0001
mdx, p = 0.10
Water intake (ml)
H
time period, p < 0.0001
Water intake (ml)
I
0.0677
% I-Home
D2 WT
D2 mdx
J
% I-Home
C57 WT
C57 mdx
K
% T-Home
D2 WT
D2 mdx
L
% I-Home
C57 WT
C57 mdx
D2 WT
D2 mdx
C57 WT
C57 mdx

Figure 3

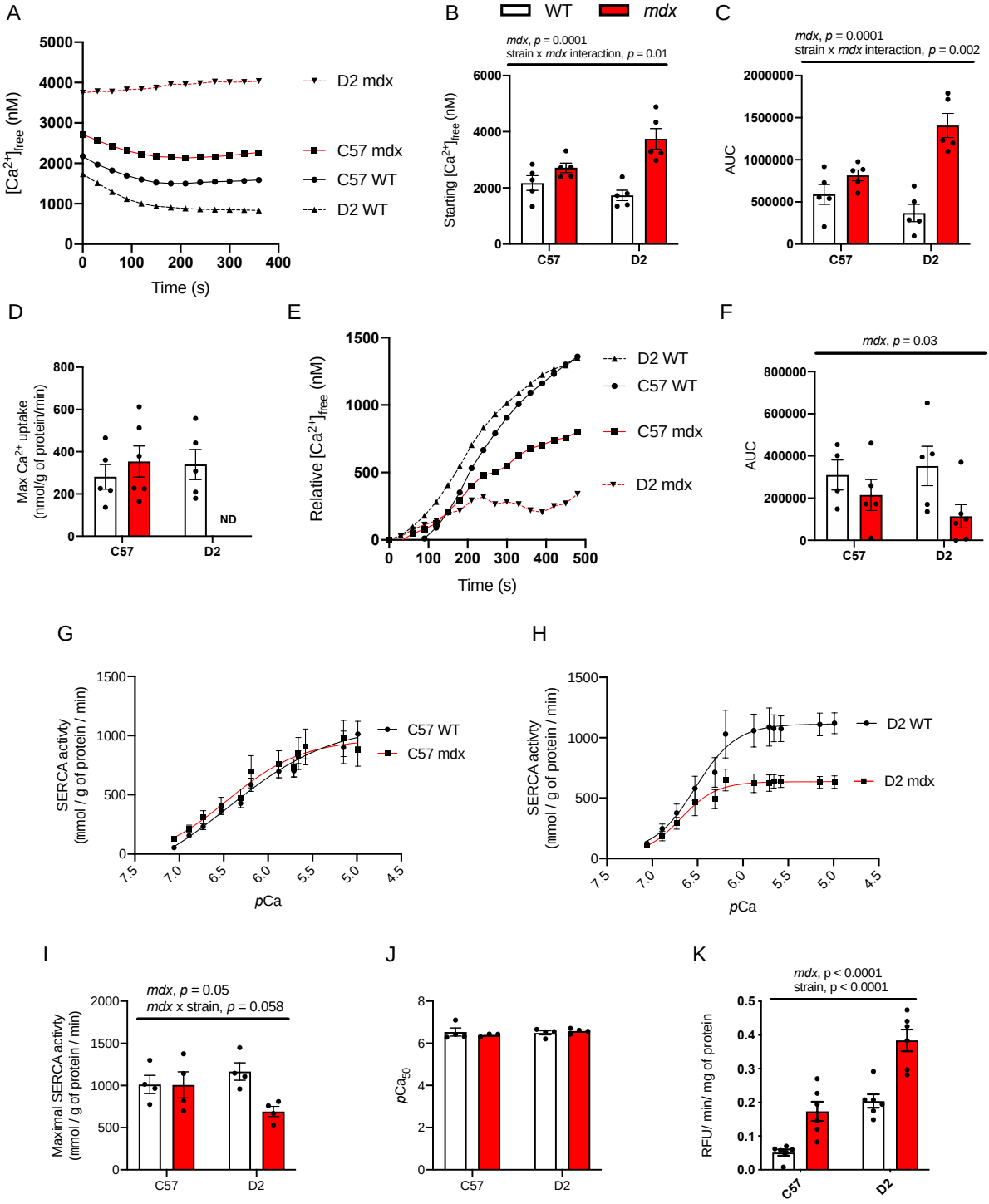
A
[Ca2+]free (nM)
Time (s)
D2 mdx
C57 mdx
C57 WT
D2 WT
B
WT
mdx
mdx, p = 0.0001
strain x mdx interaction, p = 0.01
Starting [Ca2+]free (nM)
C57
D2
C
mdx, p = 0.0001
strain x mdx interaction, p = 0.002
AUC
D
Max Ca2+ uptake (nmol/g of protein/min)
ND
E
Relative [Ca2+]free (nM)
Time (s)
F
mdx, p = 0.03
AUC
G
SERCA activty (mmol / g of protein / min)
pCa
H
I
mdx, p = 0.05
mdx x strain, p = 0.058
Maximal SERCA activty (mmol / g of protein / min)
J
pCa50
K
mdx, p < 0.0001
strain, p < 0.0001
RFU/ min/ mg of protein

Figure 4

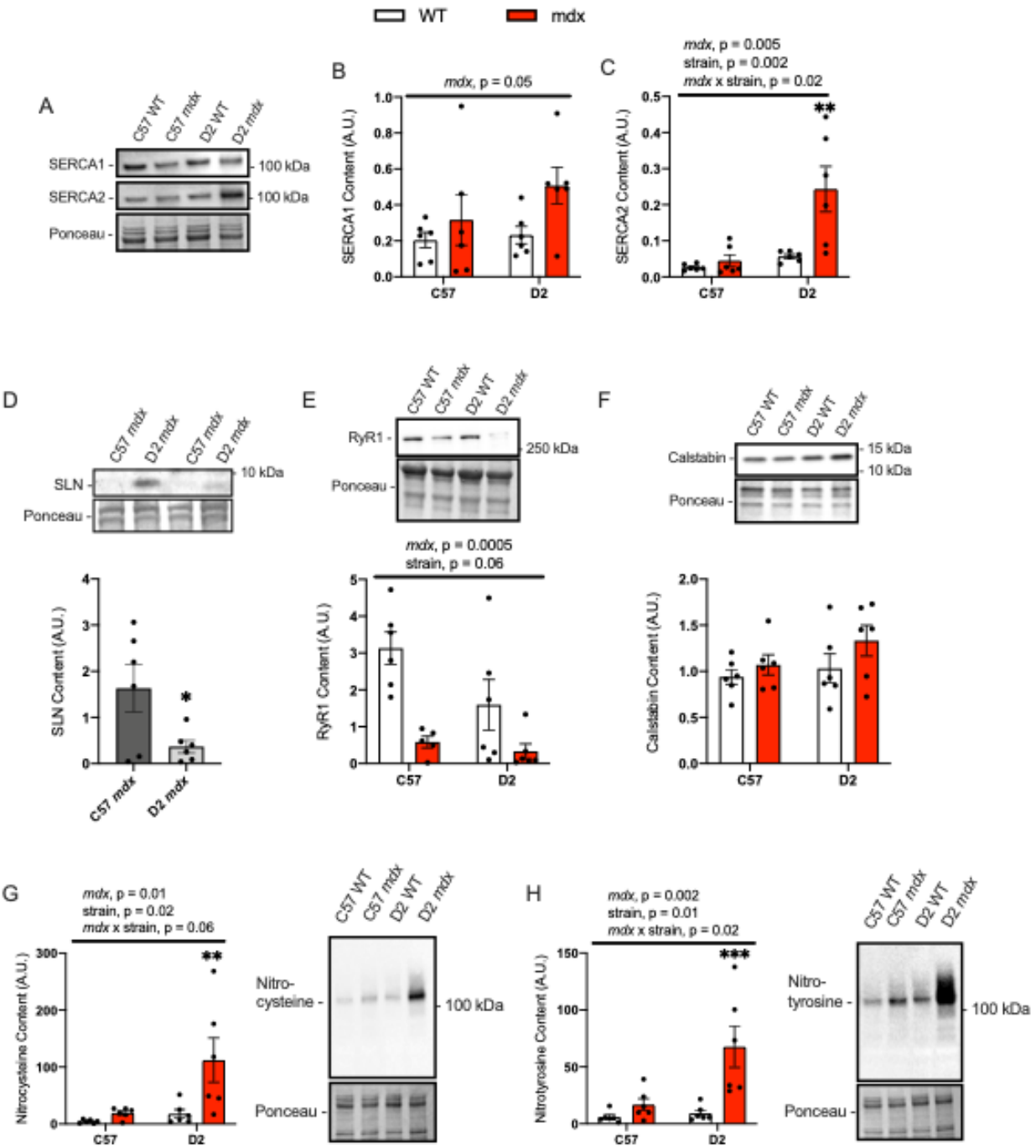
WT
mdx
A
C57 WT
C57 mdx
D2 WT
D2 mdx
SERCA1
SERCA2
Ponceau
100 kDa
100 kDa
B
mdx, p = 0.05
SERCA1 Content (A.U.)
C57
D2
C
mdx, p = 0.005
strain, p = 0.002
mdx x strain, p = 0.02
SERCA2 Content (A.U.)
D
SLN
10 kDa
SLN Content (A.U.)
E
RyR1
250 kDa
mdx, p = 0.0005
strain, p = 0.06
RyR1 Content (A.U.)
F
Calstabin
15 kDa
10 kDa
Calstabin Content (A.U.)
G
mdx, p = 0.01
strain, p = 0.02
mdx x strain, p = 0.06
Nitrocysteine Content (A.U.)
Nitro-cysteine
H
mdx, p = 0.002
strain, p = 0.01
mdx x strain, p = 0.02
Nitrotyrosine Content (A.U.)
Nitro-tyrosine

Figure 5

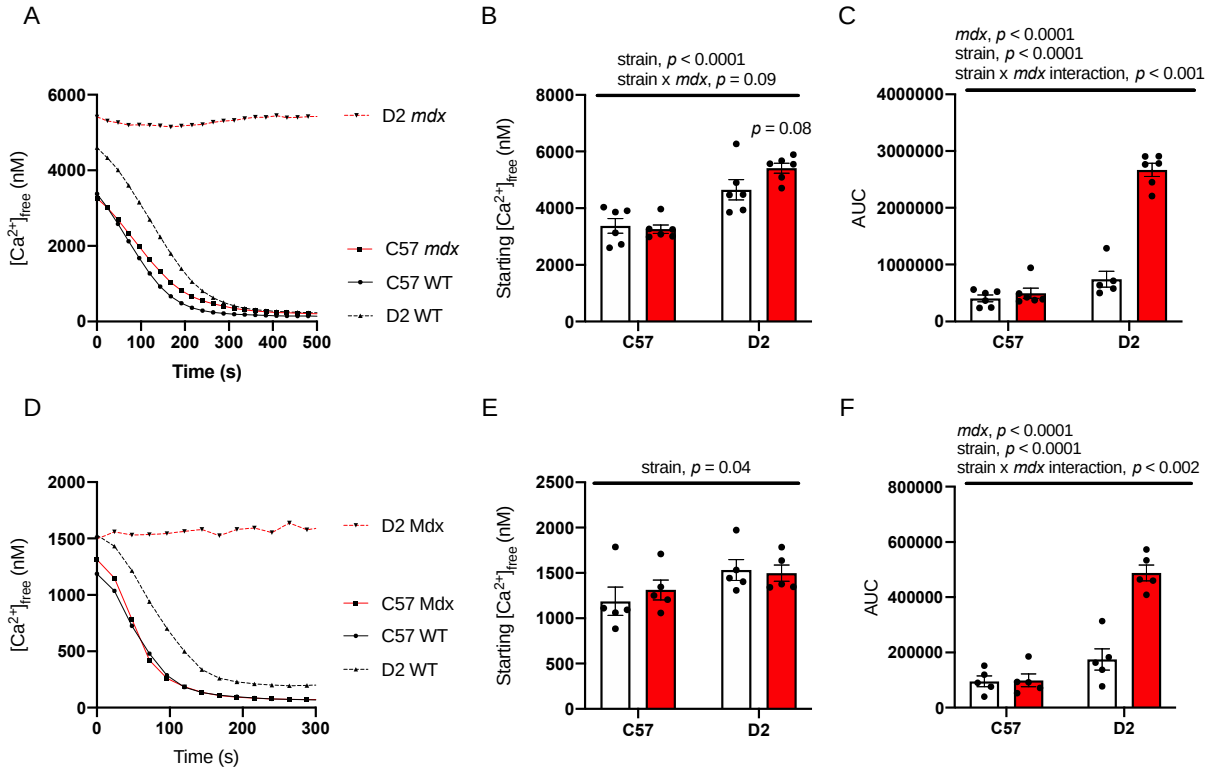
A
B
C
D
E
F
D2 mdx
C57 mdx
C57 WT
D2 WT
D2 Mdx
C57 Mdx
[Ca2+]free (nM)
Time (s)
strain, p < 0.0001
strain x mdx, p = 0.09
p = 0.08
Starting [Ca2+]free (nM)
mdx, p < 0.0001
strain, p < 0.0001
strain x mdx interaction, p < 0.001
AUC
strain, p = 0.04
mdx, p < 0.0001
strain, p < 0.0001
strain x mdx interaction, p < 0.002
C57
D2